Rotating quantum droplets confined in an anharmonic potential

S. Nikolaou,[1] G. M. Kavoulakis [ID],[1,2] and M. Ögren [ID][2,3]

[1]*Department of Mechanical Engineering, Hellenic Mediterranean University, P.O. Box 1939, 71004 Heraklion, Greece*
[2]*HMU Research Center, Institute of Emerging Technologies, 71004 Heraklion, Greece*
[3]*School of Science and Technology, Örebro University, 70182 Örebro, Sweden*

We investigate the rotational properties of quantum droplets, which form in a mixture of two Bose-Einstein condensates, in the presence of an anharmonic trapping potential. We identify various phases as the atom number and the angular momentum or angular velocity of the trap vary. These phases include center-of-mass–like excitation (without or with vortices), vortices of single and multiple quantization, etc. Finally, we compare our results with those of the single-component problem.

I. INTRODUCTION

It is well known that when a superfluid rotates, fascinating effects arise, which constitute the collection of phenomena that we call superfluidity [1]. Initial studies of superfluidity focused on homogeneous superfluids, such as in liquid helium, confined in a bucket. The great progress that has been achieved in the field of trapped atomic superfluids in the past 25 years has introduced another very important aspect of this study: the effect of the trapping potential on the rotational response of these superfluid systems.

In the initial experiments [2–8] the trapping potential was harmonic. Since the centrifugal potential scales also quadratically with the distance from the center of the trap, the rotational frequency of the trap Ω is limited by the trap frequency ω. Interestingly enough, as Ω approaches ω from below, the gas enters a highly correlated regime. This is a very interesting problem, which has attracted a great deal of attention (see, e.g., the review article of Ref. [9]).

Eventually, other forms of confining potentials were developed and studied, with the most common one being the anharmonic quartic potential. Such a potential was studied both experimentally (see, e.g., Ref. [10]) and theoretically (see, e.g., Refs. [11–19]). Contrary to the case of a harmonic confining potential, in this case there is no bound on the value of Ω. The study of this problem has shown that there is a wide variety of phases, which include vortices of single and multiple quantization, a vortex lattice with or without a hole, etc.

Another interesting aspect in the more general problem of confined superfluids under rotation is the problem of binary mixtures and their dynamics and properties. These range, for example, from the formation of magneticlike defects in binary mixtures [20], the dynamics of singly and doubly quantized composite vortices [21], and the relative dynamics of vortices and massive cores [22] to the precession inversion effect of massive vortices [23] and the stability of quantized vortices in binary condensates [24].

A recent and interesting development in the field of binary superfluid mixtures has to do with the so-called quantum droplets, whose existence was proposed by Petrov [25]. These highly quantum objects form in binary mixtures of Bose-Einstein condensed atoms. The basic idea that leads to the formation of quantum droplets is that by tuning the inter- and intra-atomic interaction strengths, the mean-field interaction energy becomes comparable to the next-order correction of the energy [26], which is essentially negligible in a single-component system (due to the assumption that we deal with dilute gases). Then the balance between the mean-field energy and the beyond-mean-field correction to the energy gives rise to self-bound quantum droplets.

This problem has recently attracted a great deal of attention (see, e.g., the review articles in [27,28] as well as Refs. [29–54]). Quantum droplets have also been observed experimentally both in mixtures of Bose-Einstein condensed gases [55–59] and in single-component gases with strong dipolar interactions [60–65].

Being self-bound, quantum droplets exist in free space and do not require the presence of any trapping potential. On the other hand, it is both experimentally and theoretically very interesting to investigate the rotational response of this new superfluid system in the presence of an external trapping potential.

Motivated by the remarks of the previous paragraphs, we investigate in the present study the rotational response of a quantum droplet under the action of an anharmonic potential [49,66]. The results of Ref. [66], which studied the same problem, are consistent with the ones presented below. On the other hand, our study demonstrates the very rich structure of this problem, since we have identified numerous distinct phases. In addition, Ref. [49] has studied the same problem, as well as the dynamics of a quantum droplet confined in an anharmonic potential.

An interesting aspect of our study arises from the comparison of the present problem, i.e., the rotational response of an anharmonically trapped quantum droplet, with that of a single-component condensate confined in the same potential. For this problem we refer to, e.g., Refs. [11–18,67–69] for a single-component condensate, as well as to Ref. [70] for the case of a binary mixture (but not in the limit where droplets form).

As we analyze below, there are some similarities but also some serious differences between the two problems. One major difference is that, while in the single-component problem there is an unstable phase (when the effective interaction is attractive), in the case of droplets such a phase is never present. In addition, in the problem of a single component, for a sufficiently small atom number, vortices of multiple quantization are always energetically favorable, independently of the sign of the effective interaction. On the other hand, in droplets, for a small atom number the motion resembles center-of-mass excitation, provided the absolute value of the energy due to the nonlinear term is much larger than the energy due to the anharmonic potential.

According to the results that we present below, there is a wide variety of phases in the problem of an anharmonically confined rotating droplet. These include center-of-mass–like excitation, with a density distribution which varies from being almost axially symmetric to being largely distorted. In addition, we find phases with vortices of single and multiple quantization, as well as a mixed phase, which is, approximately, a combination of center-of-mass and vortex excitation.

The paper is organized as follows. In Sec. II we present the model that we use. We choose to work with a fixed total angular momentum L, minimizing the energy for some fixed L, since this makes the problem more transparent. In Sec. III we present the results of our study for some representative values of the atom number of the droplet N and of the angular momentum per particle $\ell = L/N$. We identify the various phases resulting from our analysis. We also derive the function $\ell = \ell(\Omega)$ for the case where, instead of ℓ, the rotational angular velocity of the trap Ω is fixed. In Sec. IV we present the general picture that results from our analysis and derive an experimentally relevant phase diagram. In Sec. V we investigate the experimental relevance of our results, giving some typical values of the various parameters. In Sec. VI we summarize the main results of our study.

II. MODEL

Assuming that there is a very tight confining potential along the axis of rotation, we consider motion of the atoms in the perpendicular plane, i.e., two-dimensional motion. We also assume that the quantum droplet is confined in a two-dimensional anharmonic potential

$$V(\rho) = \frac{M}{2}\omega^2\rho^2\left(1 + \lambda\frac{\rho^2}{a_0^2}\right). \tag{1}$$

Here ρ is the radial coordinate in cylindrical-polar coordinates, M is the atom mass, which is assumed to be the same for the two components, ω is the frequency of the harmonic potential, $a_0 = \sqrt{\hbar/M\omega}$ is the oscillator length, and λ is a

(dimensionless) parameter which controls the strength of the anharmonic part of the trapping potential.

We consider the symmetric case, where we have equal populations of atoms $N/2$ in the two components, equal masses, and the couplings between the same components are also assumed to be equal. In this case the order parameter of the two components $\Psi_\uparrow$ and $\Psi_\downarrow$ are equal to each other, $\Psi_\uparrow = \Psi_\downarrow$.

We introduce $\Psi = \sqrt{2}\Psi_\uparrow = \sqrt{2}\Psi_\downarrow$ and also the unit of density

$$\Psi_0^2 = \frac{e^{-2\gamma-1}}{\pi}\frac{\ln(a_{\uparrow\downarrow}/a)}{aa_{\uparrow\downarrow}}. \tag{2}$$

Here a and $a_{\uparrow\downarrow}$ are the two-dimensional scattering lengths for elastic atom-atom collisions between the same species (assumed to be equal for the two components) and for different species, respectively, while γ is Euler's constant $\gamma \approx 0.5772$. Also [29],

$$\ln(a_{\uparrow\downarrow}/a) = \sqrt{\frac{\pi}{2}}\left(\frac{a_z}{a^{3D}} - \frac{a_z}{a_{\uparrow\downarrow}^{3D}}\right). \tag{3}$$

Here a_z is the width of the droplet along the axis of rotation and a^{3D} and $a_{\uparrow\downarrow}^{3D}$ are the three-dimensional scattering lengths for elastic atom-atom collisions between the same and different species, respectively. The unit of length that we adopt is

$$x_0 = \sqrt{\frac{aa_{\uparrow\downarrow}\ln(a_{\uparrow\downarrow}/a)}{4e^{-2\gamma-1}}}, \tag{4}$$

while those of the energy E_0 and of the frequency ω_0 are

$$E_0 = \hbar\omega_0 = \frac{\hbar^2}{Mx_0^2} = \frac{\hbar^2}{Maa_{\uparrow\downarrow}}\frac{4e^{-2\gamma-1}}{\ln(a_{\uparrow\downarrow}/a)}. \tag{5}$$

Finally, the number of atoms is measured in units of N_0, where

$$N_0 = \Psi_0^2 x_0^2 = \frac{1}{4\pi}\ln^2(a_{\uparrow\downarrow}/a). \tag{6}$$

In the rest of the paper we work in dimensionless units (using the units presented above), while we give some estimates for the experimentally relevant quantities in Sec. V.

We choose to work with fixed L and N, minimizing the extended energy functional [71], which (in dimensionless units) takes the form [29]

$$\mathcal{E}(\Psi, \Psi^*) = \int\left[\frac{1}{2}|\nabla\Psi|^2 + \frac{1}{2}\omega^2\rho^2\left(1 + \lambda\frac{\rho^2}{a_0^2}\right)|\Psi|^2 \right.$$
$$\left. + \frac{1}{2}|\Psi|^4\ln\frac{|\Psi|^2}{\sqrt{e}}\right]d^2\rho$$
$$- \mu\int\Psi^*\Psi\,d^2\rho - \Omega\int\Psi^*\hat{L}\Psi\,d^2\rho. \tag{7}$$

In this equation Ψ is normalized to the total number of atoms $\int|\Psi|^2d^2r = N$. Also, $\hat{L}$ is the operator of the angular momentum, while μ and Ω are Lagrange multipliers, corresponding to the conservation of the atom number and of the angular momentum, respectively. The corresponding nonlinear equation that $\Psi(\rho, \theta)$ satisfies is

$$\left[-\frac{1}{2}\nabla^2 + \frac{1}{2}\omega^2\rho^2\left(1 + \lambda\frac{\rho^2}{a_0^2}\right) + |\Psi|^2\ln|\Psi|^2 - \Omega\hat{L}\right]\Psi = \mu\Psi. \tag{8}$$

Equation (8) is solved by minimizing numerically the functional of Eq. (7), using the damped second-order-in-fictitious-time method [71], which is a method for constrained minimization. In our calculations, we use a square spatial grid, with $\delta x = \delta y = 0.1$, which proves to be accurate enough, in the sense that it produces results that are converged with respect to the grid resolution. The size of the calculational domain is larger than presented in the figures below, in order to avoid boundary effects.

We use a variety of trial order parameters as the initial condition for the calculations, namely, states that represent center-of-mass excitation, surface-wave excitation, and vortex excitation, as well as mixed states, which correspond to combinations of the aforementioned modes of excitation. The use of multiple initial conditions in the calculation, for each value of the angular momentum, and the comparison of the corresponding energies of the solutions are necessary to verify that we have reached the lowest-energy state and not some local minimum of the energy functional, which would correspond to an excited state.

III. RESULTS

Given that there are many parameters, in the derived results we consider the case where both the harmonic and the anharmonic terms in the energy are smaller than the energy that results from the nonlinear term. In the opposite limit the droplet is squeezed by the trap and the physics is, at least qualitatively, similar to the one-component system, with an effective repulsive interaction.

We have performed extensive numerical simulations and below we present some representative data for four values of $N = 50$, 100, 150 and 200, for a fixed value of $\lambda = 0.05$, and for a fixed value of $\omega = 0.05$. For a free droplet in the Thomas-Fermi limit, the radial size of the droplet ρ_0 is $\sqrt{N\sqrt{e}/\pi}$. For $N \approx 100$, which is the typical N that we use, $\rho_0 \approx 10$. On the other hand, the oscillator length $a_0 = 1/\sqrt{\omega}$ is approximately equal to 5, i.e., the two length scales are comparable (as they should be). Finally, the anharmonic term in the energy $\lambda \rho^2/a_0^2$ is on the order $\lambda \omega N$, which is somewhat less than unity.

A. Case $N = 50$

We start with a small (scaled) atom number $N = 50$. In a purely harmonic potential the center-of-mass coordinate separates from the relative coordinates and these two degrees of freedom are decoupled. More specifically, $\mathbf{R} = (1/\mathcal{N})\sum_{i=1}^{\mathcal{N}} \mathbf{r}_i$ is the center-of-mass coordinate, where $\mathcal{N}$ is the nonscaled atom number, and $\mathbf{q}_i = \mathbf{r}_i - \mathbf{R}$ are the coordinates of each particle, relative to the center of mass. The many-body state can be written in the form

$$\Psi(\mathbf{r}_1, \mathbf{r}_2, \ldots, \mathbf{r}_\mathcal{N}) = \Psi_{\text{c.m.}}(\mathbf{R}) \times \Psi_r(\mathbf{q}_1, \mathbf{q}_2, \ldots, \mathbf{q}_\mathcal{N}). \quad (9)$$

As a result, one way for the droplet to carry its angular momentum is via center-of-mass excitation, with no change in its internal structure. This is actually what happens for $N = 50$ and $\lambda = 0$ [50].

In the anharmonic potential that we consider here, the two kinds of excitation are coupled. As seen in Figs. 1(a)–1(c), we
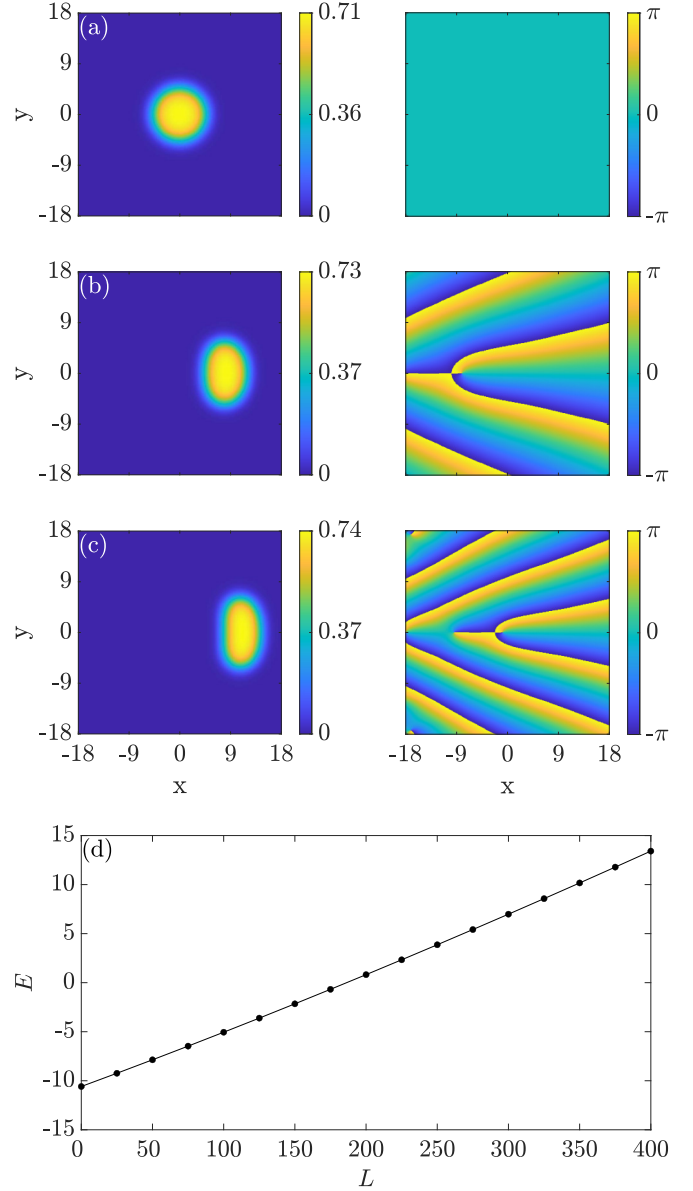

FIG. 1. (a)–(c) Density (left column) and phase (right column) of the droplet order parameter for $N = 50$, $\omega = 0.05$, $\lambda = 0.05$, and (a) $\ell = 0.0$, (b) $\ell = 4.0$, and (c) $\ell = 8.0$. Here the density is measured in units of Ψ_0^2 and the length in units of x_0. (d) Corresponding dispersion relation as a function of L. Here the energy is measured in units of E_0 and the angular momentum in units of $\hbar$.

still have a picture that resembles center-of-mass excitation; however, the droplet is also distorted from being exactly axially symmetric. This is due to the presence of the quartic term in the trapping potential, which implies that the separation between center-of-mass and relative coordinates is no longer an exact result. This coupling between the center-of-mass coordinate and the relative coordinates also manifests in the phase of the droplet, which, for $\ell \neq 0$, exhibits discontinuities, in contrast to the case of $\lambda = 0$. Here the discontinuities correspond to phantom vortices, that is, vortices in regions of space where the density is exponentially small.

Another effect of the quartic term in the confining potential is that the effective potential, i.e., the trapping plus
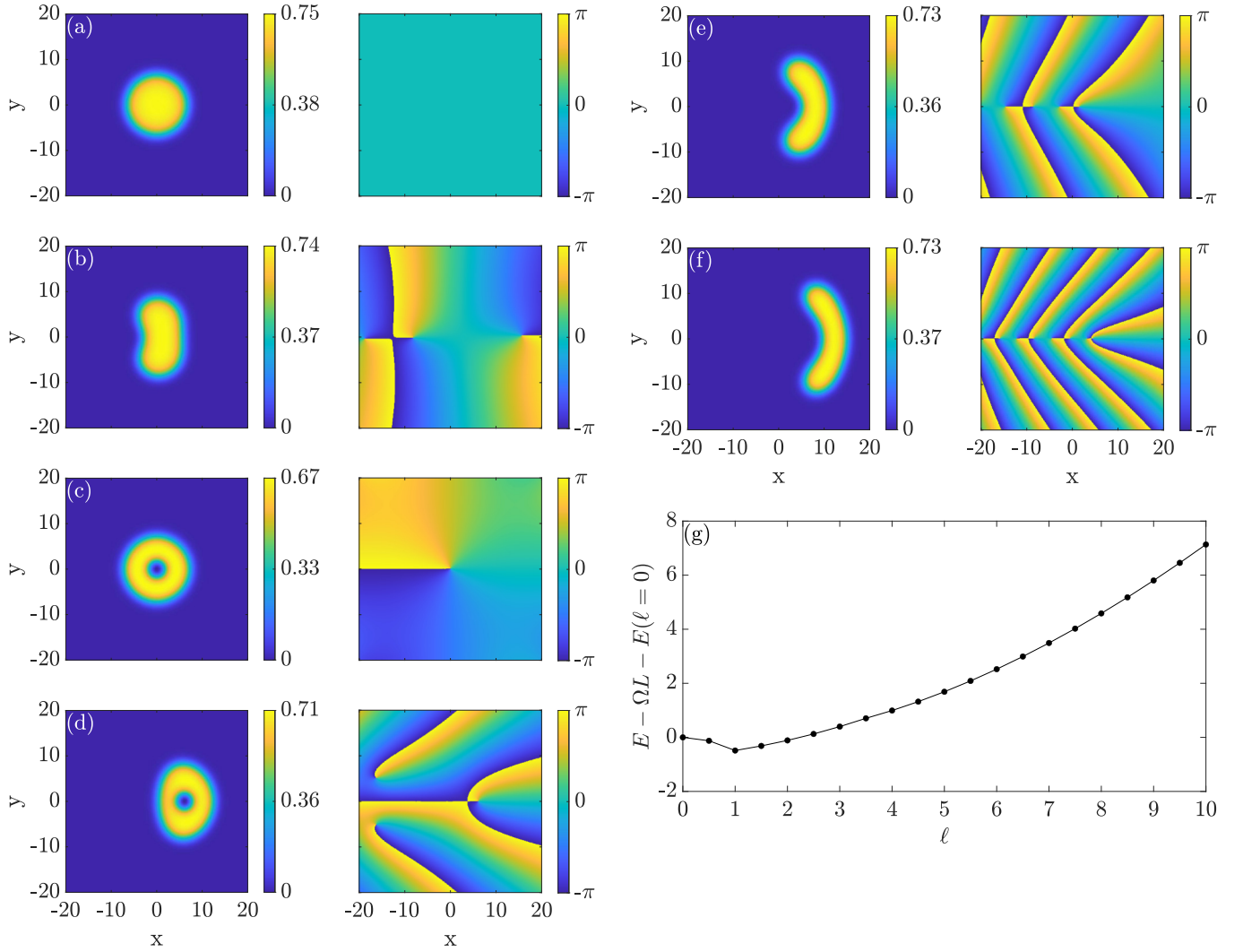
FIG. 2. (a)–(d) Density (left column) and phase (right column) of the droplet order parameter for $N = 100$, $\omega = 0.05$, $\lambda = 0.05$, and (a) $\ell = 0.0$, (b) $\ell = 0.5$, (c) $\ell = 1.0$, and (d) $\ell = 3.5$. Here the density is measured in units of Ψ_0^2 and the length in units of x_0. (e) and (f) Same as (a)–(d) but for $\ell = 4.0$, and 10.0, respectively. (g) Corresponding dispersion relation, in the rotating frame, i.e., $E_{\rm rot}(\ell) - E(\ell = 0)$ as a function of ℓ, with $\Omega = 0.054$. Here the energy is measured in units of E_0 and the angular momentum in units of $\hbar$.

the centrifugal,

$$V_{\rm eff} = V(\rho) - \frac{1}{2}\Omega^2\rho^2 = \frac{1}{2}(\omega^2 - \Omega^2)\rho^2 + \frac{\lambda}{2}\omega^2\frac{\rho^4}{a_0^2}, \quad (10)$$

takes the form of a sombrero for $\Omega > \omega$. Its minimum occurs at

$$\frac{\rho_0}{a_0} = \left[\frac{1}{2\lambda}\left(\frac{\Omega^2}{\omega^2} - 1\right)\right]^{1/2}. \quad (11)$$

For the data shown in Fig. 1, when $\ell = 4.0$, $\Omega \approx 0.060\,24$ and Eq. (11) gives $\rho_0 \approx 9.5$, while for $\ell = 8.0$, $\Omega \approx 0.065\,56$ and $\rho_0 \approx 12.0$. These values of ρ_0 coincide with the minimum of the effective potential and this is what determines the location of the droplet. As mentioned earlier, the presence of a quartic term in the potential plays a crucial role. If this is not present, for $\Omega > \omega$ there is no restoring force and the droplet would escape to infinity.

Let us turn to the dispersion relation $E(L)$, which we show in Fig. 1(d). Fitting the numerical data with a quadratic

polynomial, we find that

$$E(L) \approx -10.6032 + 0.054\,117L + 1.4911 \times 10^{-5}L^2. \quad (12)$$

We see that $E(L)$ is almost a linear function, with a slope that is higher than ω though. Also, the curvature is small and positive. These results are analyzed below.

B. Case $N = 100$

The second value of N that we consider is 100. As seen in Fig. 2, in this case the droplet carries its angular momentum in a very different way. For values of the angular momentum $0 < \ell < 1$, the droplet gets distorted due to the approach of a vortex state [Fig. 2(b)]. For $\ell = 1.0$ there is a singly quantized vortex state that is located at the center of the trap and of the droplet [Fig. 2(c)]. For higher values of ℓ, the droplet starts to move away from the center of the trap, in a mixed state, which resembles center-of-mass excitation of the vortex-carrying droplet [Fig. 2(d)]. However, this mixed state again has a density distribution that is axially asymmetric. Specifically,

the inner half of the droplet, i.e., the half closer to the origin, gets progressively more squeezed as the value of ℓ increases.

As ℓ increases even further, the situation changes completely, as shown in Figs. 2(e) and 2(f). For $\ell = 4.0$ it is no longer energetically favorable for the droplet to accommodate a vortex in the distorted mixed state. Rather, it takes advantage of the sombrero shape of the effective potential, which has a minimum at $\rho_0 \approx 9.5$ (for $\Omega \approx 0.060\,131$), while ρ_0 becomes approximately equal to 13.0 for $\ell = 10.0$ (where $\Omega \approx 0.067\,842$).

The corresponding energy, which is shown in Fig. 2(g) in the rotating frame, i.e., $E_{\text{rot}} = E(\ell) - L\Omega$ for $\Omega = 0.054$, develops some structure in this case, contrary to Fig. 1. More specifically, we see that there is a minimum for $\ell = 1$.

C. Case $N = 150$

The third value of N that we consider is 150. Here, when $0 < \ell \leqslant 1$, the picture is qualitatively the same as for $N = 100$. However, for $1 < \ell < 2$, a second vortex approaches, forming a doubly quantized vortex state for $\ell = 2.0$ [Fig. 3(a)]. For larger ℓ values, in particular $2 < \ell \leqslant 4$, the droplet exists in a mixed state, which now resembles center-of-mass–like excitation containing two singly quantized vortices [Fig. 3(b)]. Finally, for $\ell \geqslant 4.5$, the droplet forms again a localized state with center-of-mass–like excitation [Figs. 3(c) and 3(d)].

The corresponding energy, which is shown in Fig. 3(e) in the rotating frame, again develops some structure. More specifically, we see that for $\Omega = 0.054$ there is a global minimum for $\ell = 1$. For $\Omega = 0.058$, the global minimum instead shifts to $\ell = 2$.

D. Case $N = 200$

The fourth and final value of N that we consider is 200. In this case, we observe in Fig. 4 that when ℓ is sufficiently small, i.e., up to $\ell = 2.5$, the droplet carries its angular momentum via accommodating one or more singly quantized vortices [Figs. 4(b)–4(f)]. For $\ell = 3.0$ we have a triply quantized vortex state instead [Fig. 4(g)]. Essentially, as the angular momentum increases, the droplet accommodates more and more singly quantized vortices. However, as the vortices start to overlap, it becomes energetically favorable for them to merge into a multiply quantized vortex. Therefore, for $\ell = 2.0$ a doubly quantized vortex has higher energy compared to the state with two singly quantized vortices, while the opposite is true for integer values of $\ell > 2$. For $\ell = 3.5$ there are three singly quantized vortices, with an asymmetric density distribution [Fig. 4(h)]. This state belongs to the class of mixed states, which combine vortex and center-of-mass–like excitations. However, here this mode of excitation is energetically favorable only for a small range of angular momentum values. Specifically, for $\ell = 4.0$, there is again a multiply quantized vortex state with winding number equal to 4 [Fig. 4(i)]. For $\ell = 4.5$ we have phantom vortices, i.e., vortex states of single quantization at the regions of space where the density is very low, with a droplet density which is distorted [Fig. 4(j)]. For $\ell = 5.0$ there is a multiply quantized vortex state with winding number equal to 5 [Fig. 4(k)]. Interestingly enough,
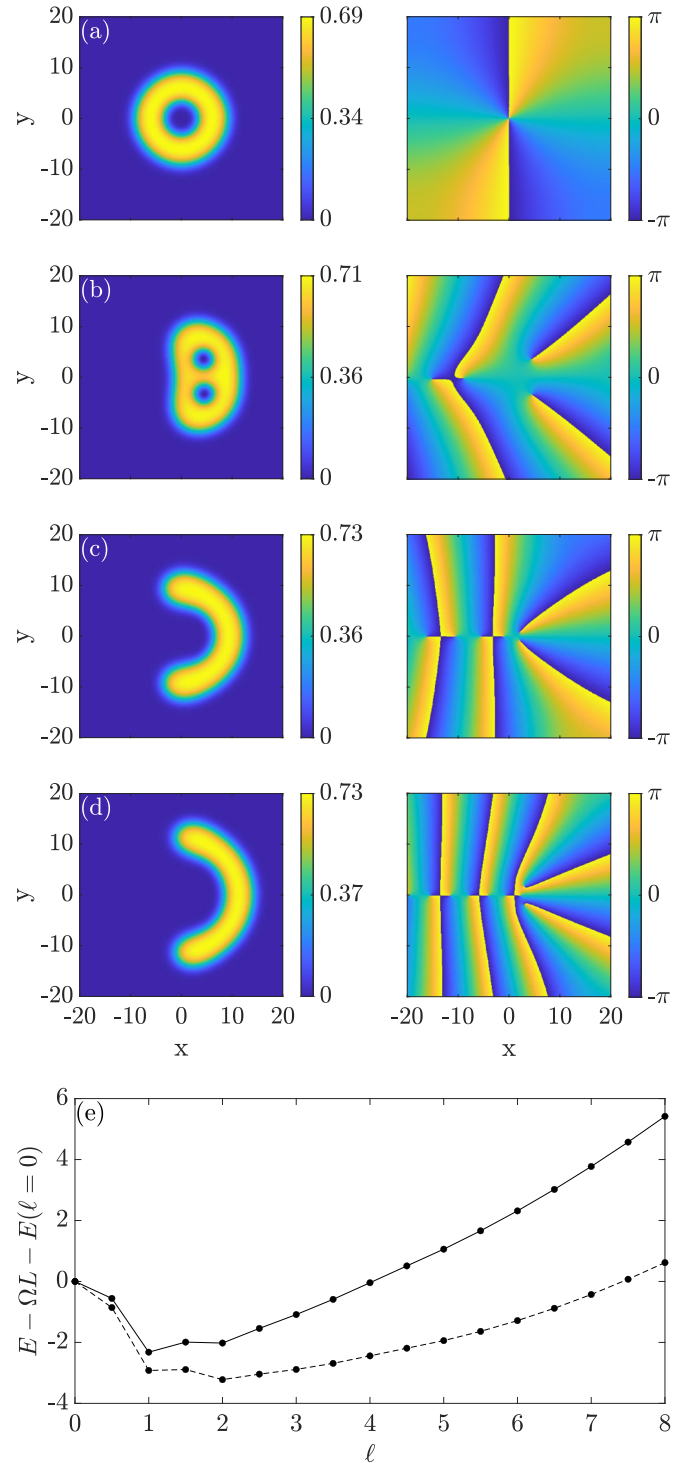

FIG. 3. (a)–(d) Density (left column) and phase (right column) of the droplet order parameter for $N = 150$, $\omega = 0.05$, $\lambda = 0.05$, and (a) $\ell = 2.0$, (b) $\ell = 3.5$, (c) $\ell = 5.0$, and (d) $\ell = 8.0$. Here the density is measured in units of Ψ_0^2 and the length in units of x_0. (e) Corresponding dispersion relation, in the rotating frame, i.e., $E_{\text{rot}}(\ell) - E(\ell = 0)$ as a function of ℓ, with $\Omega = 0.054$ (solid curve) and $\Omega = 0.058$ (dashed curve). Here the energy is measured in units of E_0 and the angular momentum in units of $\hbar$.

for $\ell = 5.5$ the droplet density breaks the axial symmetry, forming a localized blob [Fig. 4(l)]. For $\ell = 6.0$ we have a
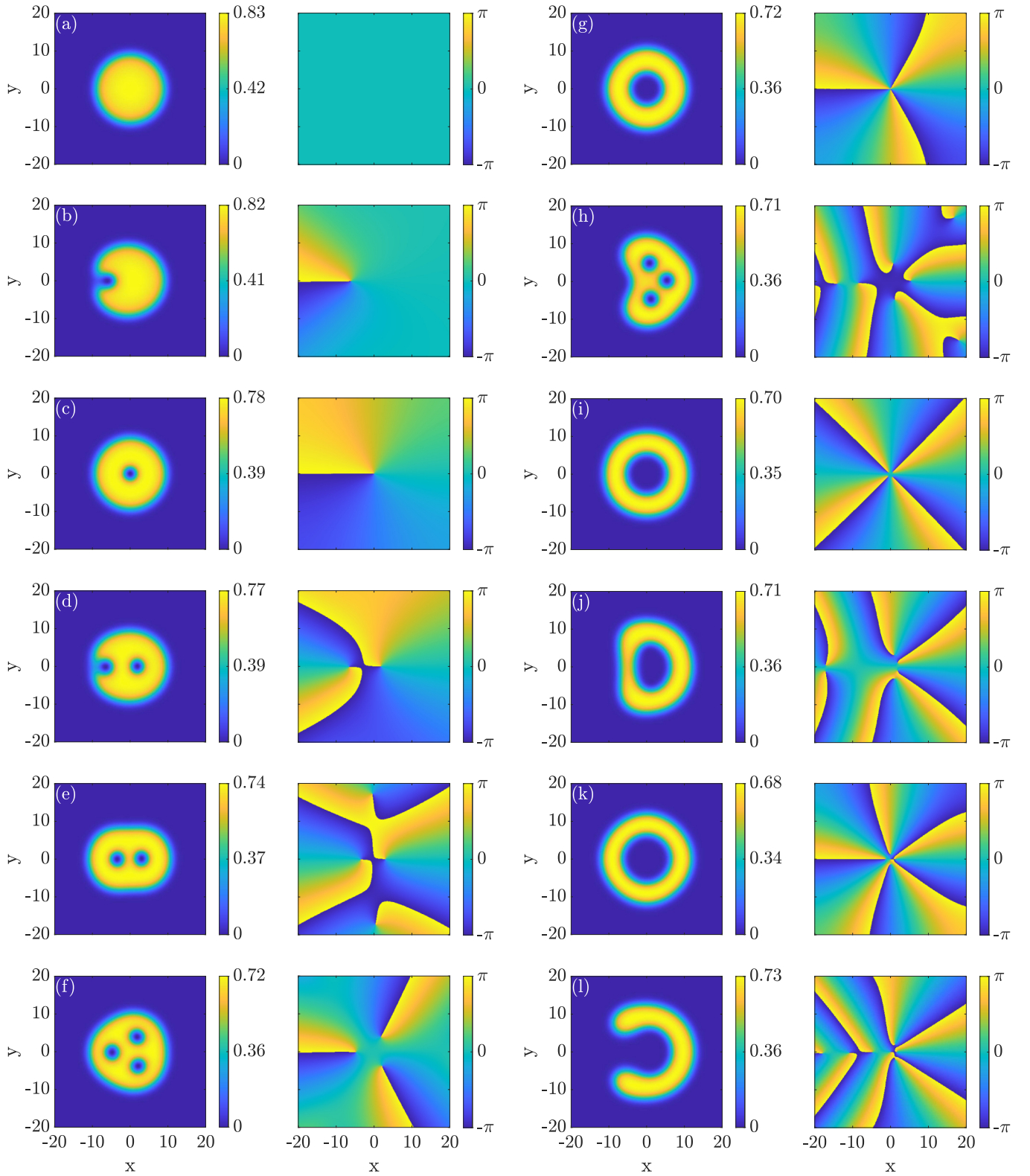
FIG. 4. (a)–(f) Density (left column) and phase (right column) of the droplet order parameter for $N = 200$, $\omega = 0.05$, $\lambda = 0.05$, and (a) $\ell = 0.0$, (b) $\ell = 0.5$, (c) $\ell = 1.0$, (d) $\ell = 1.5$, (e) $\ell = 2.0$, and (f) $\ell = 2.5$. Here the density is measured in units of Ψ_0^2 and the length in units of x_0. (g)–(l) Same as (a)–(f) but for $\ell = 3.0, 3.5, 4.0, 4.5, 5.0$, and 5.5, respectively.

multiply quantized vortex state with winding number equal to 6 [Fig. 5(a)]. Finally, for values of $\ell \geqslant 6.5$ the droplet

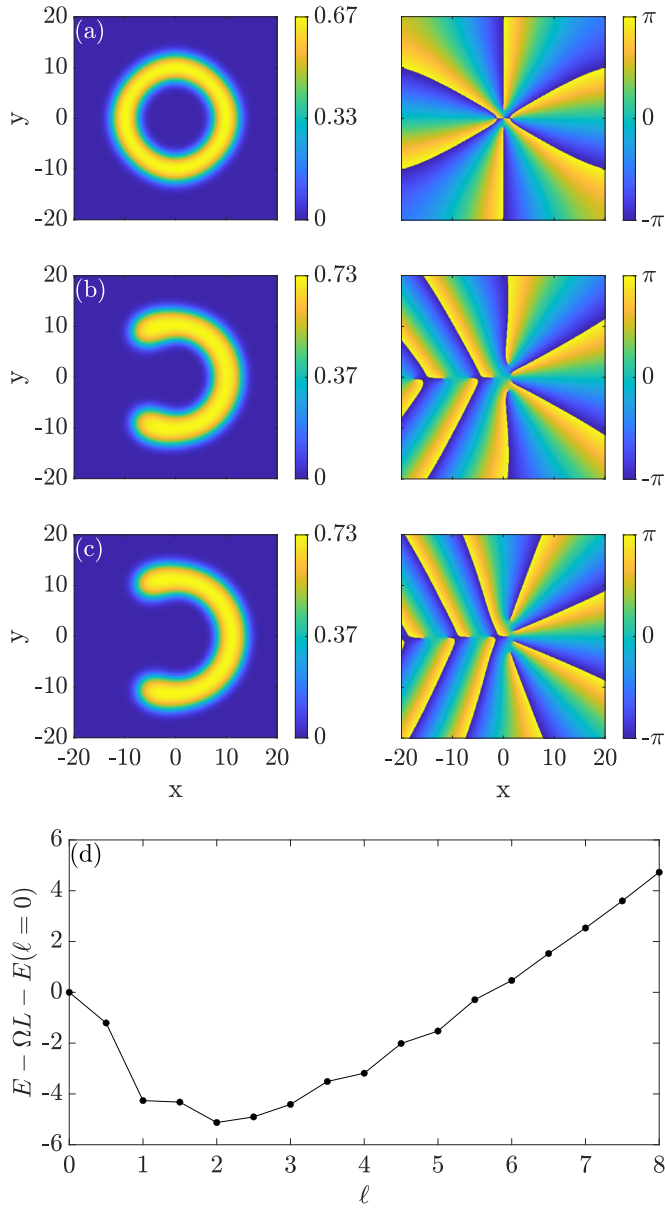forms again a localized blob along the minima of the effective potential [Figs. 5(b) and 5(c)].

FIG. 5. (a)–(c) Density (left column) and phase (right column) of the droplet order parameter for $N = 200$, $\omega = 0.05$, $\lambda = 0.05$, and (a) $\ell = 6.0$, (b) $\ell = 6.5$, and (c) $\ell = 8.0$. Here the density is measured in units of Ψ_0^2 and the length in units of x_0. (d) Corresponding dispersion relation, in the rotating frame, i.e., $E_{\mathrm{rot}}(\ell) - E(\ell = 0)$ as a function of ℓ, with $\Omega = 0.054$. Here the energy is measured in units of E_0 and the angular momentum in units of $\hbar$.

The energy $E(\ell)$ shown in Fig. 5(d) in the rotating frame for $\Omega = 0.054$ develops an even more interesting structure as compared to Figs. 1 and 2. Depending on the value of Ω, this function has minima for various values of ℓ, as is clear in Fig. 6(d).

E. Fixing Ω instead of L

Up to now, all the calculations that we have performed are for fixed angular momentum. From the derived dispersion relation $E(\ell)$ one may also see how the droplet would respond if Ω is fixed instead. This is done by considering the energy
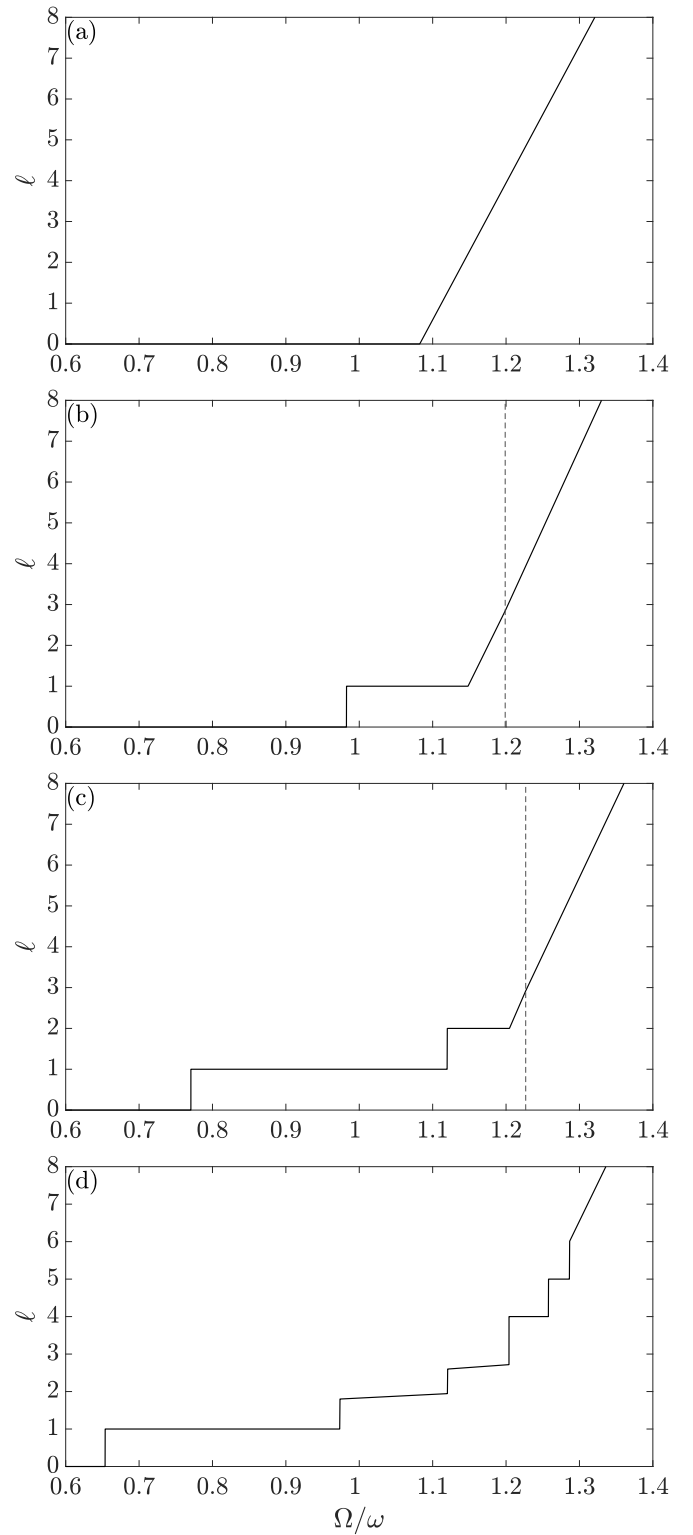

FIG. 6. Function $\ell = \ell(\Omega)$ for the four values of (a) $N = 50$, (b) $N = 100$, (c) $N = 150$, and (d) $N = 200$ that we consider. Dashed vertical lines denote a transition from a mixed state to a localized state (see the text for details). Here the angular momentum is measured in units of $\hbar$.

in the rotating frame, i.e., $E_{\mathrm{rot}} = E(\ell) - \Omega L$, and locating the minimum. This is how Fig. 6 is derived, where we show the function $\ell = \ell(\Omega)$ for $N = 50, 100, 150$, and 200.

For the smallest value $N = 50$, we see that the droplet undergoes center-of-mass–like excitation (see Fig. 1). As a result, for fixed Ω, there is a critical value of this frequency below which the droplet does not respond and is static. This critical value is $\Omega \approx 0.054\,117$ (equivalently, $\Omega/\omega \approx 1.08$), i.e., it is the coefficient of the linear term in Eq. (12), as expected. When Ω exceeds this value, the angular momentum starts to increase linearly with Ω, as seen in Fig. 6(a), according to the classical expression $L = I\Omega$, where I is the moment of inertia of the droplet.

For $N = 100$ the picture changes (see Fig. 2), as seen in Fig. 6(b). In this case, there is again a critical value of Ω below which the droplet is static; however, when Ω exceeds this value, the droplet undergoes a discontinuous (due to the negative curvature of the dispersion relation for $0 < \ell < 1$) transition to a state with a vortex that is located at its center. As Ω increases further, the droplet undergoes a transition to a mixed state, where $\ell = \ell(\Omega)$ is a linear function. Finally, the droplet transitions to a localized state, where we have center-of-mass–like excitation. Again, in this case $\ell = \ell(\Omega)$ is a linear function, according to the classical formula $L = I\Omega$. For $N = 150$ [Fig. 6(c)] the picture is essentially similar (see Fig. 3), with the addition of an extra step in $\ell = \ell(\Omega)$, located at $\ell = 2$.

It is important to note here that in the $\ell = \ell(\Omega)$ plot, $N = 100$ and 150 each manifests two linear regions, i.e., with different slopes, one corresponding to mixed excitation and one corresponding to center-of-mass–like excitation. However, we stress that the difference between these two slopes, for each value of N, is minuscule. As a result, the linear regions for $N = 100$ and 150 appear to be uniform in Figs. 6(b) and 6(c).

Finally, for $N = 200$, a richer picture, as compared to $N = 100$ and 150, emerges (see Figs. 4 and 5). One difference is that the critical value of Ω for the entry of the first vortex decreases. Another difference is that there are more steps in $\ell = \ell(\Omega)$, before the droplet (again) gets to a localized state, where (again) we have center-of-mass–like excitation. Here there is no linear part corresponding to mixed excitation, i.e., no mixed state appears as an energy minimum in the rotating frame. The formula $L = I\Omega$ also holds here.

A general observation about the center-of-mass–like excitation is that, while the formula $L = I\Omega$ is always valid, with increasing N, the value of I increases too. As a result, the slope of the linear part of the plotted functions increases as N increases, as seen throughout Figs. 6(a)–6(d).

An interesting observation regards the order of transition to the mixed states. For $N = 100$, the transition from the singly quantized vortex state to the mixed state is continuous. Conversely, for $N = 150$, the transition from the doubly quantized vortex state to the mixed state is discontinuous, i.e., first order.[1] The discontinuity here arises from the negative

curvature of the dispersion relation for $2 < \ell \lesssim 3$. We stress that, when needed, we use a step in the ℓ values that is smaller than 0.5 (which is used in the plots of the dispersion relations), down to 0.01, so that we can accurately determine the curvature and therefore the order of transitions.

We can also comment on the order of transition to the localized states with center-of-mass–like excitation. For $N = 50$, the transition from the static droplet to center-of-mass–like excitation is continuous. However, for $N = 100$, 150, and 200 the transition to a localized state is discontinuous. In particular, for $N = 100$ and 150 there is a level crossing between the branch of the mixed states and the branch of center-of-mass–like excitation. This level crossing is located at $\Omega \approx 0.059\,94$ for $N = 100$ and at $\Omega \approx 0.061\,34$ for $N = 150$, corresponding to the dashed vertical lines in Figs. 6(b) and 6(c).

IV. GENERAL PICTURE OF THE PHASE DIAGRAM

From the results that are presented in the previous sections, it is clear that the problem we have considered has a very rich structure. In this section we give some general features of the phase diagram that includes the rotational frequency of the trap on the one axis and the atom number on the other axis, concentrating on the states which minimize the energy in the rotating frame.

As mentioned also earlier, we have considered the case where both the harmonic and the anharmonic terms in the energy are smaller than the energy that results from the nonlinear term. In the opposite limit the droplet is squeezed by the trap and the physics is, at least qualitatively, similar to the one-component system, with an effective repulsive interaction. This is due to the fact that when the density exceeds (sufficiently) the density of the droplet in free space, the nonlinear term becomes (predominantly) positive.

Figure 7 shows the phase diagram, where the data correspond to the ones presented in Sec. III E. For a sufficiently small atom number N, the only phase that is present, for all values of Ω, is the one which resembles center-of-mass excitation. This is due to the fact that for the assumed small value of N the droplet size is also small and is not affected by the presence of the trapping potential.

As N increases, i.e., as we move vertically in the phase diagram, the droplet expands radially and starts to get squeezed by the external trapping potential. As a result, the nonlinear term becomes predominantly repulsive. Furthermore, the energy due to both the harmonic and the anharmonic parts of the trapping potential increases. As a result, the system no longer undergoes center-of-mass–like excitation, but rather it supports vortex states, either of multiple or of single quantization (for even larger values of N). Although not presented in this work, we have even identified another mixed phase, for sufficiently large values of N, which contains a hole, i.e., a multiply quantized vortex, at the center of the droplet and singly quantized vortices around it. This phase has also been identified in anharmonically confined, rotating Bose-Einstein condensates with effectively repulsive contact interactions [18].

---

[1]Here there also exists a continuous transition, from the doubly quantized vortex state to a mixed state, with center-of-mass–like excitation of the doubly quantized vortex. However, this particular mixed state is an excited state, similar to the excited states identified in Ref. [50] but with an axially asymmetric density distribution.
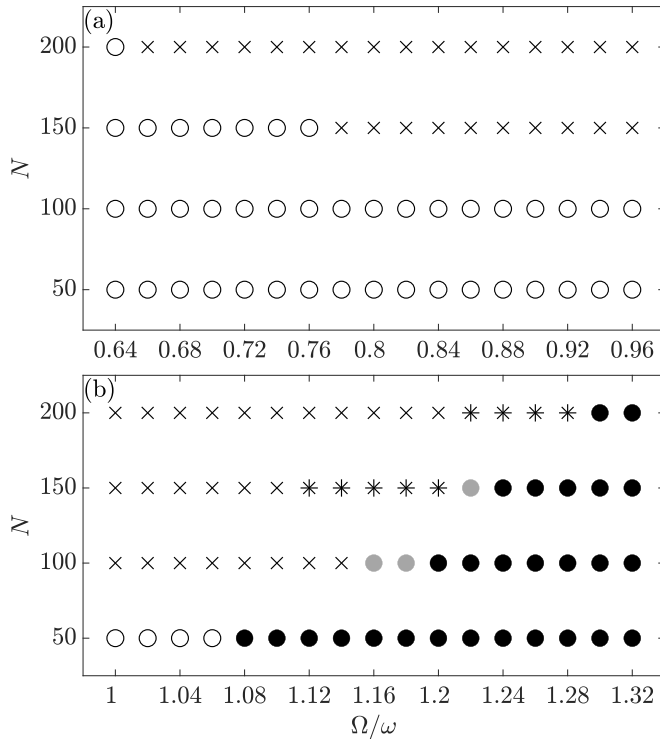
FIG. 7. Various phases that we have derived, on the $\Omega/\omega - N$ plane, which correspond to the absolute minima of the energy in the rotating frame (see Sec. III E), for (a) slow and (b) rapid rotation. On the horizontal axis is Ω/ω and on the vertical is N. Here different phases are denoted by the following symbols: $\bigcirc$, the nonrotating ground state; $\times$, vortices of single quantization or vortex lattices; $\ast$, vortices of multiple quantization; $\newcommand\graycircle{}$ ●, the mixed phase (see the text for details); and ●, the center-of-mass–like localized state.

For a fixed atom number and with increasing Ω, i.e., as we move horizontally in the phase diagram, the physics of the droplet is determined by the effective potential, which has a sombrero shape for $\Omega > \omega$. Then the droplet forms either vortices of multiple quantization or a localized blob around the minimum of the effective potential, in a state which breaks the axial symmetry of the Hamiltonian.

V. EXPERIMENTAL RELEVANCE

So far we have been working with dimensionless units for convenience. Here we give some numbers which relate to the physical units and allow one to make a connection with actual experiments.

For a typical value of $a_z = 0.1$ μm, $a^{3D} = 10.1$ nm, $a_{\uparrow\downarrow}^{3D} = -10.0$ nm, and $\ln(a_{\uparrow\downarrow}/a) \approx 25$. Then, according to Eq. (6), $N_0 \approx 50$. Therefore, the range of N that we consider (50 up to 200) corresponds roughly to approximately 2500, up to approximately 10 000 atoms in an experiment.

Also, the unit of length x_0 turns out to be on the order of 1 μm. This implies that, for, e.g., 10^4 atoms, the size of a (nonrotating) droplet in the Thomas-Fermi limit, which was evaluated in Sec. III, is approximately equal to 10 μm. A typical value of the two-dimensional density is approximately equal to 10^9 cm^{-2}, a typical value of the three-dimensional density is 10^{13} cm^{-3}, the unit of time t_0 is on the order of

milliseconds, and the typical value of ω is hundreds of hertz. Finally, a typical value of the anharmonicity parameter λ is approximately equal to 10^{-2} [10].

Although the Hamiltonian of the problem we consider is axially symmetric, many of the solutions that we find break this axial symmetry, which is an example of spontaneous symmetry breaking.

The case where Ω is fixed is probably more relevant experimentally. In this case one makes the implicit assumptions that there is an infinitesimally weak asymmetry in the trapping potential and that the system has enough time to equilibrate in the rotating frame. We stress that such weak asymmetries in the trapping potential are essentially unavoidable. Regarding the equilibration in the rotating frame, this is mainly related to the timescale of the lifetime of the atoms in the trap.

As long as the asymmetry in the trap is infinitesimally weak, the phases that we derive will remain unaffected. In this case, the only effect of the asymmetry is to "assist" the system reach the state that breaks the axial symmetry. On the other hand, in the presence of a strong asymmetry the problem is very different and is beyond the scope of the present work.

VI. SUMMARY

In the present paper we investigated the rotational properties of a mixture of two Bose-Einstein condensates, which consists of equal populations of distinguishable atoms having equal masses. Under the further assumption that the mean-field energy of this binary mixture is sufficiently small, the next-order correction to the energy is non-negligible (as opposed to most other cases) and the balance between the two terms results in the formation of quantum droplets.

The presence of an (even weak) anharmonic term in the potential has very serious consequences on the rotational response of the gas. First of all, for a fixed rotational frequency Ω, while in a harmonic potential Ω cannot exceed ω, here there is no such restriction. Furthermore, while in a harmonic potential the center-of-mass coordinate separates from the relative coordinates, here this is no longer true.

Given that droplets are self-bound states, for a sufficiently weak trapping potential and/or a sufficiently small atom number N, the nonlinear term is attractive. The droplet then carries its angular momentum in a state that resembles center-of-mass excitation (with some distortion, though, since, as we mentioned in the preceding paragraph, the center-of-mass coordinate does not separate from the relative coordinates). As the trapping potential becomes stronger and/or the atom number N increases, the nonlinear term becomes (predominantly) repulsive. In this case, it becomes energetically favorable for the droplet to accommodate vortices either of multiple or of single quantization.

The above results are in contrast to the case of a single component, where in the limit of a weak trapping potential and/or a sufficiently small atom number N one always has vortices of multiple quantization (and this is actually true for both signs of the effective interaction). For a fixed atom number and with increasing Ω, the droplet forms either vortices of multiple quantization or a localized blob around the minimum

of the effective potential, in a state which breaks the axial symmetry of the Hamiltonian (depending on the actual value of the atom number).

We conclude by stressing that, given that in actual experiments there are always deviations from a perfectly harmonic trap, the assumption of an anharmonic potential is probably more realistic and more experimentally relevant as compared to a model of rotating quantum droplets in a purely harmonic potential. Clearly, this adds more value to the results of the present study.

[1] A. J. Leggett, Rev. Mod. Phys. **71**, S318 (1999).

[2] M. R. Matthews, B. P. Anderson, P. C. Haljan, D. S. Hall, C. E. Wieman, and E. A. Cornell, Phys. Rev. Lett. **83**, 2498 (1999).

[3] B. P. Anderson, P. C. Haljan, C. E. Wieman, and E. A. Cornell, Phys. Rev. Lett. **85**, 2857 (2000).

[4] K. W. Madison, F. Chevy, W. Wohlleben, and J. Dalibard, Phys. Rev. Lett. **84**, 806 (2000).

[5] J. R. Abo-Shaeer, C. Raman, J. M. Vogels, and W. Ketterle, Science **292**, 476 (2001).

[6] P. C. Haljan, I. Coddington, P. Engels, and E. A. Cornell, Phys. Rev. Lett. **87**, 210403 (2001).

[7] P. Engels, I. Coddington, P. C. Haljan, V. Schweikhard, and E. A. Cornell, Phys. Rev. Lett. **90**, 170405 (2003).

[8] T. W. Neely, E. C. Samson, A. S. Bradley, M. J. Davis, and B. P. Anderson, Phys. Rev. Lett. **104**, 160401 (2010).

[9] N. R. Cooper, Adv. Phys. **57**, 539 (2008).

[10] V. Bretin, S. Stock, Y. Seurin, and J. Dalibard, Phys. Rev. Lett. **92**, 050403 (2004).

[11] A. L. Fetter, Phys. Rev. A **64**, 063608 (2001).

[12] E. Lundh, Phys. Rev. A **65**, 043604 (2002).

[13] K. Kasamatsu, M. Tsubota, and M. Ueda, Phys. Rev. A **66**, 053606 (2002).

[14] U. R. Fischer and G. Baym, Phys. Rev. Lett. **90**, 140402 (2003).

[15] G. M. Kavoulakis and G. Baym, New J. Phys. **5**, 51 (2003).

[16] E. Lundh, A. Collin, and K.-A. Suominen, Phys. Rev. Lett. **92**, 070401 (2004).

[17] A. Aftalion and I. Danaila, Phys. Rev. A **69**, 033608 (2004).

[18] A. D. Jackson, G. M. Kavoulakis, and E. Lundh, Phys. Rev. A **69**, 053619 (2004).

[19] A. L. Fetter, B. Jackson, and S. Stringari, Phys. Rev. A **71**, 013605 (2005).

[20] A. Gallemí, L. P. Pitaevskii, S. Stringari, and A. Recati, Phys. Rev. A **97**, 063615 (2018).

[21] P. Kuopanportti, S. Bandyopadhyay, A. Roy, and D. Angom, Phys. Rev. A **100**, 033615 (2019).

[22] A. Bellettini, A. Richaud, and V. Penna, Eur. Phys. J. Plus **138**, 676 (2023).

[23] V. P. Ruban, JETP Lett. **115**, 415 (2022).

[24] S. Patrick, A. Gupta, R. Gregory, and C. F. Barenghi, Phys. Rev. Res. **5**, 033201 (2023).

[25] D. S. Petrov, Phys. Rev. Lett. **115**, 155302 (2015).

[26] T. D. Lee, K. Huang, and C. N. Yang, Phys. Rev. **106**, 1135 (1957).

[27] F. Böttcher, J.-N. Schmidt, J. Hertkorn, K. S. H. Ng, S. D. Graham, M. Guo, T. Langen, and T. Pfau, Rep. Prog. Phys. **84**, 012403 (2021).

[28] Z.-H. Luo, W. Pang, B. Liu, Y.-Y. Li, and B. A. Malomed, Front. Phys. **16**, 32201 (2021).

[29] D. S. Petrov and G. E. Astrakharchik, Phys. Rev. Lett. **117**, 100401 (2016).

[30] Y. Li, Z. Luo, Y. Liu, Z. Chen, C. Huang, S. Fu, H. Tan, and B. A. Malomed, New J. Phys. **19**, 113043 (2017).

[31] G. E. Astrakharchik and B. A. Malomed, Phys. Rev. A **98**, 013631 (2018).

[32] Y. V. Kartashov, B. A. Malomed, L. Tarruell, and L. Torner, Phys. Rev. A **98**, 013612 (2018).

[33] A. Cidrim, F. E. A. dos Santos, E. A. L. Henn, and T. Macrí, Phys. Rev. A **98**, 023618 (2018).

[34] P. Zin, M. Pylak, T. Wasak, M. Gajda, and Z. Idziaszek, Phys. Rev. A **98**, 051603(R) (2018).

[35] F. Ancilotto, M. Barranco, M. Guilleumas, and M. Pi, Phys. Rev. A **98**, 053623 (2018).

[36] Y. Li, Z. Chen, Z. Luo, C. Huang, H. Tan, W. Pang, and B. A. Malomed, Phys. Rev. A **98**, 063602 (2018).

[37] L. Parisi, G. E. Astrakharchik, and S. Giorgini, Phys. Rev. Lett. **122**, 105302 (2019).

[38] Y. V. Kartashov, B. A. Malomed, and L. Torner, Phys. Rev. Lett. **122**, 193902 (2019).

[39] X. Zhang, X. Xu, Y. Zheng, Z. Chen, B. Liu, C. Huang, B. A. Malomed, and Y. Li, Phys. Rev. Lett. **123**, 133901 (2019).

[40] M. N. Tengstrand, P. Stürmer, E. Ö. Karabulut, and S. M. Reimann, Phys. Rev. Lett. **123**, 160405 (2019).

[41] B. Liu, H.-F. Zhang, R.-X. Zhong, X.-L. Zhang, X.-Z. Qin, C. Huang, Y.-Y. Li, and B. A. Malomed, Phys. Rev. A **99**, 053602 (2019).

[42] R. Tamil Thiruvalluvar, S. Sabari, K. Porsezian, and P. Muruganandam, Physica E **107**, 54 (2019).

[43] G. Ferioli, G. Semeghini, S. Terradas-Briansó, L. Masi, M. Fattori, and M. Modugno, Phys. Rev. Res. **2**, 013269 (2020).

[44] I. Morera, G. E. Astrakharchik, A. Polls, and B. Juliá-Díaz, Phys. Rev. Res. **2**, 022008(R) (2020).

[45] L. Parisi and S. Giorgini, Phys. Rev. A **102**, 023318 (2020).

[46] M. Tylutki, G. E. Astrakharchik, B. A. Malomed, and D. S. Petrov, Phys. Rev. A **101**, 051601(R) (2020).

[47] P. Examilioti and G. M. Kavoulakis, J. Phys. B: At. Mol. Opt. Phys. **53**, 175301 (2020).

[48] Y. Hu, Y. Fei, X.-L. Chen, and Y. Zhang, Front. Phys. **17**, 61505 (2022).

[49] S.-C. Cheng, Y.-W. Wang, and W.-H. Kuan, arXiv:2302.07481.

[50] S. Nikolaou, G. M. Kavoulakis, and M. Ögren, Phys. Rev. A **108**, 053309 (2023).

[51] Q. Gu and X. Cui, Phys. Rev. A **108**, 063302 (2023).

[52] T. A. Yoğurt, U. Tanyeri, A. Keleş, and M. Ö. Oktel, Phys. Rev. A **108**, 033315 (2023).

[53] T. A. Flynn, N. A. Keepfer, N. G. Parker, and T. P. Billam, Phys. Rev. Res. **6**, 013209 (2024).

[54] X. Du, Y. Fei, X.-L. Chen, and Y. Zhang, Phys. Rev. A **108**, 033312 (2023).

[55] C. Cabrera, L. Tanzi, J. Sanz, B. Naylor, P. Thomas, P. Cheiney, and L. Tarruell, Science **359**, 301 (2018).

[56] P. Cheiney, C. R. Cabrera, J. Sanz, B. Naylor, L. Tanzi, and L. Tarruell, Phys. Rev. Lett. **120**, 135301 (2018).

[57] G. Semeghini, G. Ferioli, L. Masi, C. Mazzinghi, L. Wolswijk, F. Minardi, M. Modugno, G. Modugno, M. Inguscio, and M. Fattori, Phys. Rev. Lett. **120**, 235301 (2018).

[58] G. Ferioli, G. Semeghini, L. Masi, G. Giusti, G. Modugno, M. Inguscio, A. Gallemí, A. Recati, and M. Fattori, Phys. Rev. Lett. **122**, 090401 (2019).

[59] C. D'Errico, A. Burchianti, M. Prevedelli, L. Salasnich, F. Ancilotto, M. Modugno, F. Minardi, and C. Fort, Phys. Rev. Res. **1**, 033155 (2019).

[60] H. Kadau, M. Schmitt, M. Wenzel, C. Wink, T. Maier, I. Ferrier-Barbut, and T. Pfau, Nature (London) **530**, 194 (2016).

[61] M. Schmitt, M. Wenzel, F. Böttcher, I. Ferrier-Barbut, and T. Pfau, Nature (London) **539**, 259 (2016).

[62] I. Ferrier-Barbut, H. Kadau, M. Schmitt, M. Wenzel, and T. Pfau, Phys. Rev. Lett. **116**, 215301 (2016).

[63] I. Ferrier-Barbut, M. Schmitt, M. Wenzel, H. Kadau, and T. Pfau, J. Phys. B: At. Mol. Opt. Phys. **49**, 214004 (2016).

[64] I. Ferrier-Barbut, M. Wenzel, F. Böttcher, T. Langen, M. Isoard, S. Stringari, and T. Pfau, Phys. Rev. Lett. **120**, 160402 (2018).

[65] L. Chomaz, S. Baier, D. Petter, M. J. Mark, F. Wächtler, L. Santos, and F. Ferlaino, Phys. Rev. X **6**, 041039 (2016).

[66] L. Dong and Y. V. Kartashov, Phys. Rev. Lett. **126**, 244101 (2021).

[67] A. D. Jackson and G. M. Kavoulakis, Phys. Rev. A **70**, 023601 (2004).

[68] G. M. Kavoulakis, A. D. Jackson, and G. Baym, Phys. Rev. A **70**, 043603 (2004).

[69] A. Collin, E. Lundh, and K.-A. Suominen, Phys. Rev. A **71**, 023613 (2005).

[70] E. Ö. Karabulut, F. Malet, G. M. Kavoulakis, and S. M. Reimann, Phys. Rev. A **87**, 043609 (2013).

[71] M. Gulliksson and M. Ögren, J. Phys. A: Math. Theor. **54**, 275304 (2021).